TEM investigation of hot pressed -10 vol.%SiC–ZrB_2 composite

D. D. Jayaseelan*[1], Y. Wang[1], G. E. Hilmas[2], W. Fahrenholtz[2], P. Brown[3] and W. E. Lee[1]

The polytypism of SiC, phase transformation of ZrB_2 and the interfaces between SiC and ZrB_2 were investigated using high resolution TEM in a hot pressed 10 vol.%SiC-ZrB_2 composite. In most cases, no grain boundary interphases between hexagonal ZrB_2 and *6H*-SiC phases were observed with SiC being both inter- and intragranular. Occasionally, *6H*-SiC transformed into *3C* and *15R* and hexagonal ZrB_2 transformed into cubic ZrB. High resolution TEM showed no grain boundary interphases in most regions. Energy dispersive X-ray spectroscopy and electron energy-loss spectroscopy analyses showed the presence of oxygen throughout the sample. The phase transformation of SiC and ZrB_2, and the interphase formation between SiC and ZrB_2 grains are discussed.

Keywords: UHTC's, Interphases, Dislocations, ZrB_2, SiC, Microstructure

Introduction

The cornerstone of ultrahigh temperature ceramics (UHTC) is a small group of diboride and carbide ceramic–matrix composites including ZrB_2–SiC,[1–6] HfB_2–SiC,[7–9] ZrC–SiC,[10–12] HfC–SiC,[13,14] and ZrB_2–SiC–C.[15,16] They have a unique set of material properties including unusually high thermal conductivity that makes them particularly well suited for sharp body applications in hypersonic flows.[17] However, their use has been limited due to poor fracture toughness,[2,3,18–21] moderate thermal shock[3,22–25] and oxidation behaviour[4,26–30] and inability to make them fully dense. Previous evaluation of these materials suggested that their poor properties were due to agglomerates, inhomogeneities and grain boundary impurities, all of which were believed to be associated with ceramic processing problems.[31–34]

Among UHTCs, ZrB_2 has the lowest theoretical density (6·09 g cm^{-3}), which makes it attractive for aerospace applications.[35] Its high melting temperature, good thermal shock and oxidation resistance and relatively low cost when compared with HfB_2 based ceramics make it more attractive than other non-oxide structural ceramics.[35] Often, SiC is added to ZrB_2 to enhance its oxidation resistance and limit grain growth during densification.[33,35–38] Additions of up to 30 vol.%SiC particulates have been found to improve the four-point bend strength of ZrB_2 from ~565 to ~1089 MPa and fracture toughness from 3·5 to 5·25 MPa $m^{1/2}$ by limiting grain growth and promoting crack deflection.[39,40]

In recent years, significant progress has been made in densification and characterisation of Zr and Hf based UHTCs. Surprisingly, few reports appear in the literature of microstructural defects in grains or at interfaces using transmission electron microscopy (TEM). Therefore, in this paper we report an investigation of phase transformations of SiC and ZrB_2 and the interphase formation between ZrB_2 and SiC in 10 vol.%SiC–ZrB_2 composites sintered by hot pressing.

Experimental

Materials and methods

ZrB_2 powder (~98·5%, d_{50}≈2 μm, 0·2%C, 0·9%O, 0·2%Hf, grade B; HC Starck, Newton, MA, USA) and SiC powder (α-SiC, 98·5%, d_{50}≈0·7 μm, grade UF-10; HC Starck) were used as the starting materials. Phase analysis by X-ray diffraction (XRD) and using selected area electron diffraction (SAED) patterns confirm that both ZrB_2 and SiC have a hexagonal structure with lattice parameters of a=3·17 Å, c=3·53 Å and a=3·08 Å, c=15·12 Å respectively. To reduce particle size and promote intimate mixing, batches of composition 90 vol.-%ZrB_2 and 10 vol.-%SiC were attrition milled (model 01-HD; Union Process, Akron, OH, USA). Milled powders were hot pressed (model HP-3060; Thermal Technology, Santa Rosa, CA, USA) into graphite dies lined with graphite foil and coated with BN. The hot press furnace was heated at an average rate of ~5°C min^{-1} to 1900°C at ~17°C min^{-1} with simultaneous application of 32 MPa load in flowing argon. After 45 min the sample was cooled at

[1]Centre for Advanced Structural Ceramics Department of Materials, Imperial College, London SW7 2AZ, UK
[2]Department of Materials Science and Engineering, Missouri Institute of Science and Technology, Rolla, MO 65409, USA
[3]Metallics Team, Physical Sciences Department, Defense Science and Technology Laboratory, Wiltshire SP4 0JQ, UK

*Corresponding author, email d.j.daniel@imperial.ac.uk

Received 10 February 2010; accepted 26 April 2010
DOI 10.1179/174367510X12722693956310

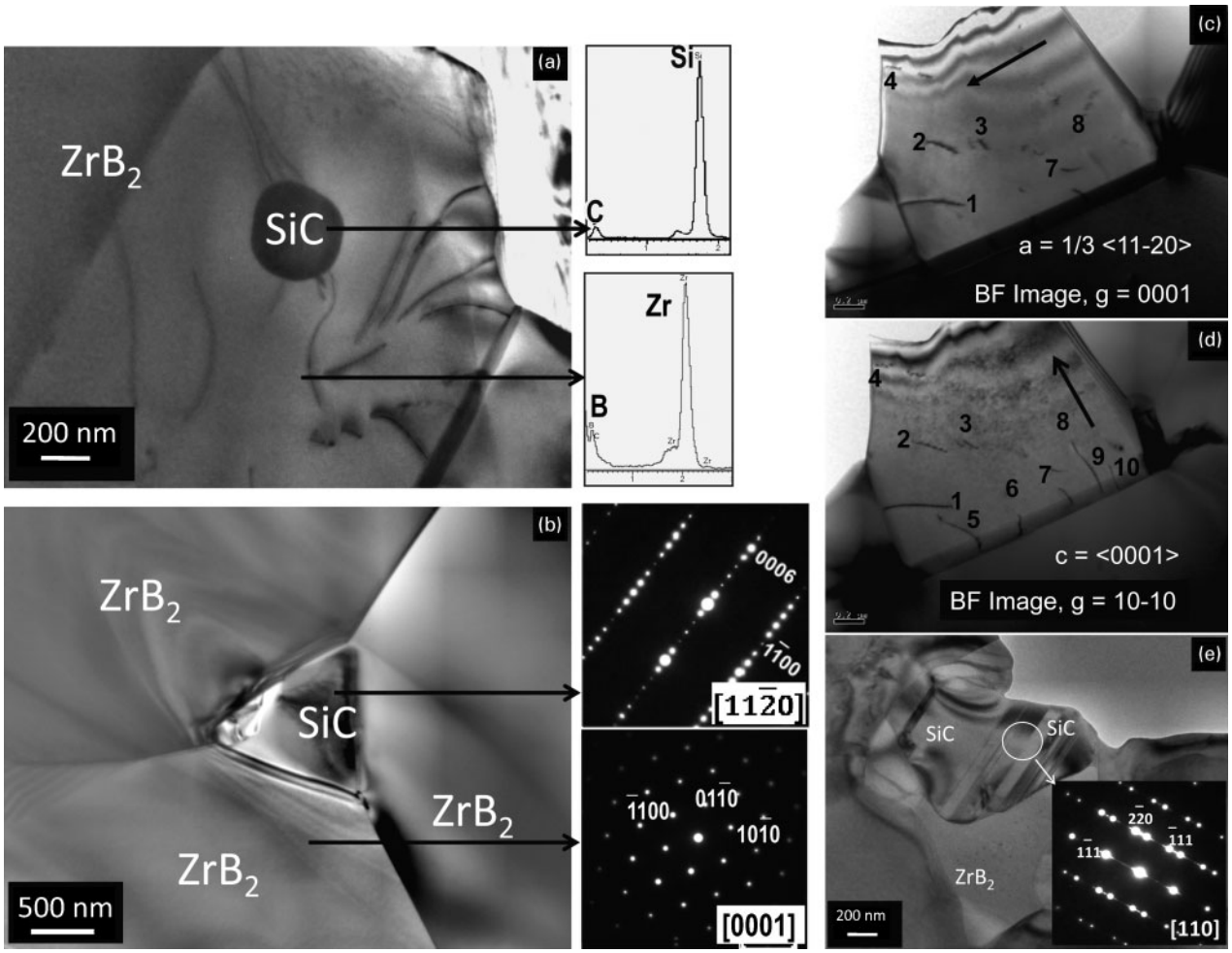

1 Typical BF images of 10 vol.%SiC-ZrB_2 composite, *a* intragranular spheroidal SiC, inset showing EDS spectra from SiC and ZrB_2; *b* intergranular SiC at ZrB_2 grain triple junction, inset showing [11–20] zone axis pattern from SiC and [0001] pattern from ZrB_2; *c* BF image showing dislocations in ZrB_2 grain originating from the grain boundary with g=0001; *d* BF image showing dislocations with g=10$\bar{1}$0; *e* SiC grain with striped contrast, inset showing [110] zone axis SAED pattern taken from circled area

$\sim$20°C min^{-1} to room temperature. Each billet is $\sim$40 mm in diameter and $\sim$5 mm in thickness. More details of the hot pressing procedure are given by Zimmermann *et al.*[39]

Characterisation by TEM

Specimens for TEM observation were prepared from hot pressed materials using conventional mechanical polishing and ion thinning. The ion thinning was performed using a Gatan model 691 precision ion polishing system. Bright field (BF) images and SAED patterns were acquired using a JEOL JEM-2000EX electron microscope operating at 200 kV. The Burgers vectors **b** of dislocations were determined using the relation **g•b**=0, where **g** is the diffraction vector. High resolution TEM (HRTEM), energy dispersive X-ray spectroscopy (EDS) and electron energy loss spectroscopy (EELS) were carried out using an FEI Titan 80–300 scanning transmission electron microscope operating at 300 kV.

Results and discussion

Figure 1 shows typical BF images of the morphologies of different phases and the interfaces in the composites. Figure 1*a* clearly reveals small (0·4 μm), intragranular spheroidal SiC grains within (about 2–3 μm sized) ZrB_2 grains containing dislocations some of which appear to be associated with the intragranular SiC. Figure 1*b* reveals an intergranular SiC at a ZrB_2 triple junction. The inset SAED pattern is a [11$\bar{2}$0] zone axis revealing that the SiC is the 6H polytype. ZrB_2 is often observed to have a hexagonal symmetry. The dislocations observed in ZrB_2 around SiC in Fig. 1*a* are most likely caused by thermal expansion mismatch between ZrB_2 (*P6/mmm*) (Ref. 41) and SiC ($P6_3mc$) (Ref. 42) grains. Figure 1*c–d* shows bright field images of a ZrB_2 grain in direct contact with a SiC grain. Diffraction contrast imaging of the dislocations in ZrB_2 has been performed under two-beam conditions using different diffraction vectors (**g**=0001 and **g**=10$\bar{1}$0). Arrows indicate the direction of **g**. Dislocations are observed to originate at the grain boundary interfaces. The dislocation Burgers vectors are determined to be either $\mathbf{a}=\frac{1}{3}\langle 11\bar{2}0\rangle$ in Fig. 1*c* or $\mathbf{c}=\langle 0001\rangle$ in Fig. 1*d* using **g•b** criteria. Figure 1*e* shows a BF image of ZrB_2–SiC composite. The grain with striped contrast is SiC. The inset in Fig. 1*e* shows the [110] zone axis SAED pattern taken from the circled area, which can be indexed as β-SiC with a zinc blende structure (*3C*-SiC). The characteristic

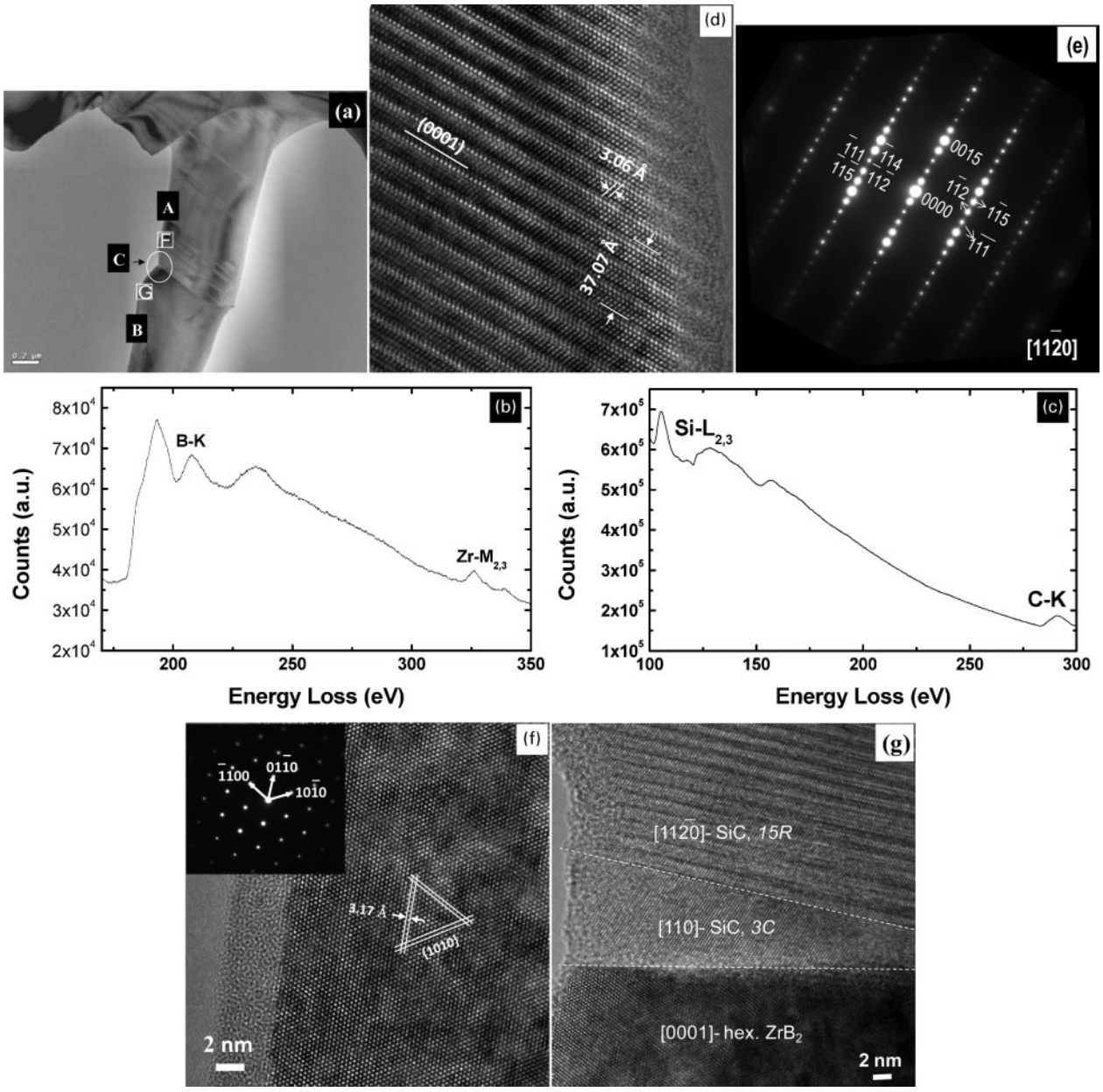

2 *a* BF image of ZrB_2/SiC interface, *b*, *c* EELS spectra acquired from region B and A respectively, *d* typical HRTEM image from region A, showing *15R*-SiC polytype, *e* corresponding [11$\bar{2}$0] zone axis SAED pattern, *f* HRTEM image taken from region B, inset showing [0001] zone axis SAED pattern and *g* HRTEM image of ZrB_2/SiC interface

double diffraction spots and streaks in the SAED pattern reveal the presence of twins and stacking faults, respectively.[43–45] No appreciable grain growth occurred during hot pressing as SiC and ZrB_2 grain sizes remain the same as those of the initial particles.

Grains with similar features are observed throughout the microstructure. Figure 2*a* shows a typical BF image of a ZrB_2/SiC interface. Analysis using EELS (Figs. 2*b* and *c*) confirms the striped region A is SiC while region B is ZrB_2. Figure 2*e* shows an HRTEM image taken down the [11$\bar{2}$0] zone axis from the area F in the SiC grain. The SAED pattern obtained from this grain (Fig. 2*e*) can only be indexed as *15R*-SiC. Careful examination of the SAED pattern reveals streaks between the diffraction spots, which indicate the presence of stacking faults in the *15R*-SiC. The HRTEM image reveals a superlattice structure with *c* parameter fifteen times that of the *3C*-SiC polymorph. The lattice parameters of *15R*-SiC are determined to be a=3·06 Å and c=37·07 Å. As can be seen from Fig. 2*d* the ideal structure of *15R*-SiC has an 'ABCACBCABACABCA' or $(3{\cdot}2)_3$ sequence.

Figure 2*f* shows a HRTEM image at the [0001] zone axis taken from the area G in the ZrB_2 grain. The inset shows the corresponding SAED pattern which can be indexed using the lattice parameters of hexagonal ZrB_2. The planar spacings for {10$\bar{1}$0} are measured to be 3·17 Å which matches that of hexagonal ZrB_2. Thus, the chemical composition, SAED pattern and the HRTEM image of region B confirm that it is hexagonal ZrB_2 which has undergone no phase transformation on processing. SiC is commonly observed in this composite: intragranular (Fig. 1*a*), intergranular (Fig. 1*b*) and with faulted contrast (Figs. 1*e* and 2*a*). The striped features in

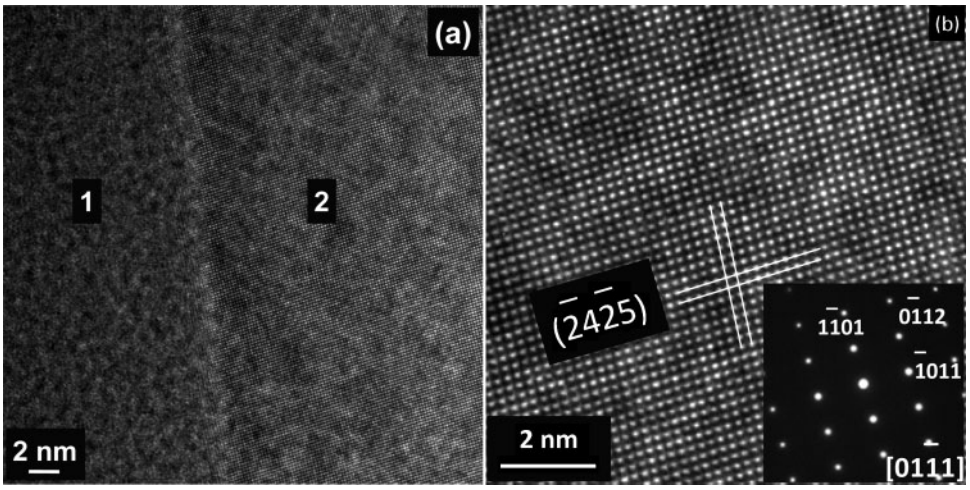

3 ***a*** **HRTEM image of ZrB_2/ZrB_2 interface and** ***b*** **enlarged HRTEM image of grain 2 showing hexagonal structure corresponding to zone axis [0 1 $\bar{1}$ 1]**

the SiC grain are attributed to planar defects such as twins and stacking faults.

High resolution TEM was performed to clarify the nature of the grain boundary between SiC and ZrB_2 in Fig. 2*a*. Figure 2*g* shows the HRTEM image taken from area C in Fig. 2*a* around the interface. Figure 2*g* shows an atomically flat and coherent interface between SiC and ZrB_2. It is observed that the grain boundary is clean and does not contain any secondary phases. Furthermore, the region of A in Fig. 2*a* closer to the SiC/ZrB_2 interface shown as *3C* in Fig. 2*g* reveals a 2·49 Å lattice spacing and the atomic arrangements show cubic structure. The lattice parameter is calculated to be a=4·32 Å from the HRTEM image. Since EELS analysis confirms the presence of only Si and C. This region is confirmed as *3C*, i.e., β SiC (a=4·35 Å). The slightly smaller lattice parameter may be caused by the strain around the interface.

Figure 2*g* shows two distinct interfaces between *15R*-SiC and *3C*-SiC, *3C*-SiC and hexagonal ZrB_2. The crystallographic orientation relationships between these interfaces were determined from Fig. 2*g*. The crystallographic orientation relationship between *15R*- and *3C*-SiC is $[11\bar{2}0]\|\|[110]$ and $(0001)\|(111)$. However, the crystallographic orientation relationship between *3C*-SiC and ZrB_2 is $[110]\|\|[0001]$ and $(111)\|(10\bar{1}0)$. In this orientation, the $(10\bar{1}0)$ planes of the hexagonal structure (ZrB_2) and the (111) planes of the cubic structure (*3C*-SiC) have minimal misfit and the strain can be accommodated more easily. The crystallographic orientation relationships of $[11\bar{2}0]\|\|[110]$ and $(0001)\|(111)$ are commonly observed for interfaces between a hexagonal and cubic phases.[46–48]

Figure 3 shows an HRTEM image of a ZrB_2/ZrB_2 interface in the ZrB_2–SiC composite. Grain 2 can be tilted to $[01\bar{1}1]$ zone axis perpendicular to (–24–25) plane, while grain 1 cannot be tilted to a low index zone axis. This means that there is no preferential orientation relationship between these two grains. A closer look at the HRTEM image of the ZrB_2/ZrB_2 interface reveals that no secondary glassy or crystalline interphases are present.

Figure 4*a* shows an HRTEM image of a further interface in the ZrB_2–SiC composite. Both grains 1 and 2 can be tilted to respective zone axes which indicates that they have crystallographic orientation relation between them. Although EDS analyses (Fig. 4*b*) reveal the presence of Zr and B in both grains, quantification of EDS spectra indicates that the composition of these two grains is different. In grain 1 the atomic ratio of Zr/B is close to 1 : 2, while in grain 2 the atomic ratio of Zr/B is close to 1 : 1. Selected area electron diffraction and HRTEM also confirm the phase differences. Figure 4*c* shows an enlarged HRTEM image of grain 2. The atomic arrangement clearly reveals it to be a cubic structure with a planar spacing of 2·69 Å for the {111} plane. As ZrB_2 is only known to exist in hexagonal form, the existence of ZrB_2 is unlikely and also the planar spacing of grain 2 does not match any of the SiC polytypes. In addition, the SAED pattern taken from grain 2 (not shown) can be indexed using a lattice parameter of a cubic phase (4·65 Å). As zirconium boride has another two cubic phases ZrB (a=4·65 Å) and ZrB_{12} (a=7·40 Å), taking into account the EDS quantification results, lattice parameter, and the crystal structure, grain 2 is most likely to be cubic ZrB. This observation suggests that a small amount (perhaps ~1 vol%) hexagonal ZrB_2 transforms into cubic ZrB during the hot pressing.

Figure 5 shows a typical BF and HRTEM image of a three-grain junction having two interfaces. Grains C and B in Figure 5*a* have similar contrast while grain A has slightly darker contrast. Grain A occurs as an intergranular phase between the two large grains. Analysis using EDS confirms that the small grain is SiC and the larger grains are ZrB_2. Selected area electron diffraction of the large grains reveals that the ZrB_2 grains are hexagonal while SAED of the small grain reveals it as *3C*-SiC. Figure 5*b* shows an HRTEM image of the interface between grain A and grain B revealing a thin 3–6 nm amorphous layer. Analysis of this interphase using EDS reveals Si and O, suggesting an amorphous silica layer forms the interphase at the grain boundary. Although XRD did not detect the presence of oxides or any other secondary phases, EDS and EELS analyses always show the presence of oxygen throughout the sample. The presence of oxygen in the sintered samples is due to its presence in the starting materials.

In this study, uncharacteristic SiC features have been observed including the transformation from α (*6H*) to β

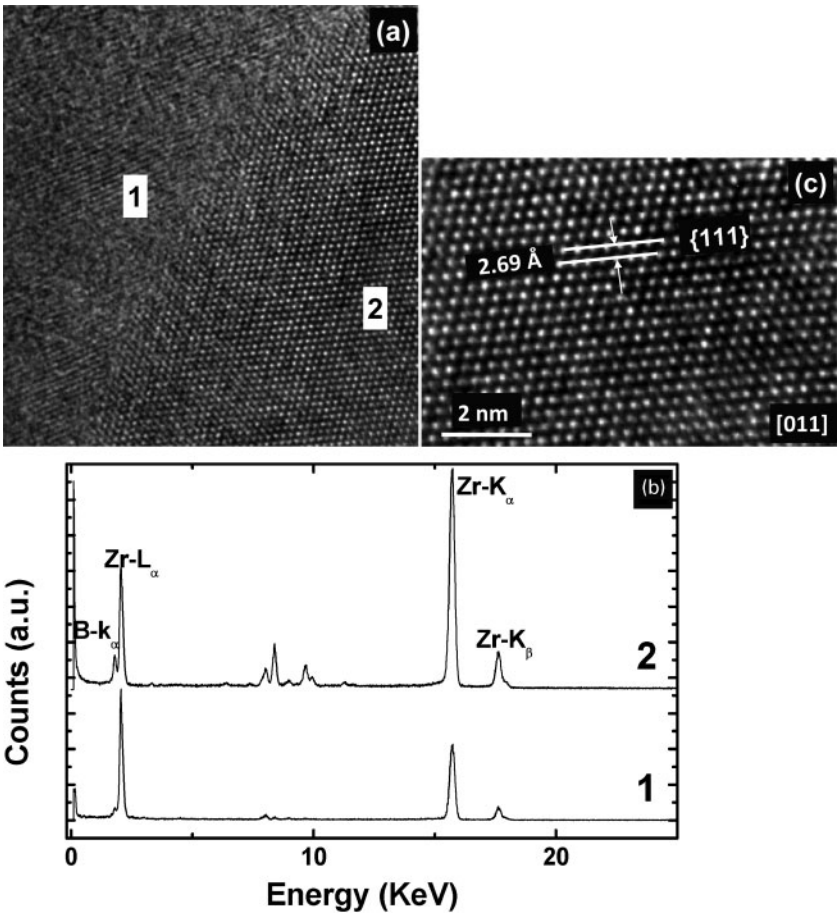

4 ***a*** **HRTEM image of ZrB_2/ZrB interface,** ***b*** **EDS analyses of grains 1 and 2 and** ***c*** **enlarged HRTEM image of grain 2 showing cubic structure corresponding to [011] zone axis**

(*3C*) polytypes. The more usual transformation is β- to α-SiC which is thermodynamically not reversible. Only Kieffer *et al.*[49] have observed *6H*- to *3C*-SiC transformation in microcrystalline powder at 2800 K when annealed for 4 h in vacuum. An *ab initio* study on the polytypic transformation suggests that a dislocation mechanism may be responsible for the temperature and deformation induced transitions.[50] Calculated energy barriers for *6H*→*3C* make the dislocation mechanism highly favourable for polytypic transformations in SiC.[50] The dislocation based polytypic transformation[51] results from the strength of the compression applied to *6H* during hot pressing. In addition, other impurities such as carbon, silicon or oxygen stabilise the *3C*-SiC structure.[52]

Another interesting feature is the transformation of ZrB_2 into ZrB. Champion *et al.*[46–48,53] studied the Zr/ZrB_2 interface and observed ZrB as the grain boundary interphase. Electron diffraction also showed the existence of ZrB cubic phase at the metal/ceramic interface and in some ZrB_2 grains. The proposed phase diagram[53] also suggested a peritectoid transformation

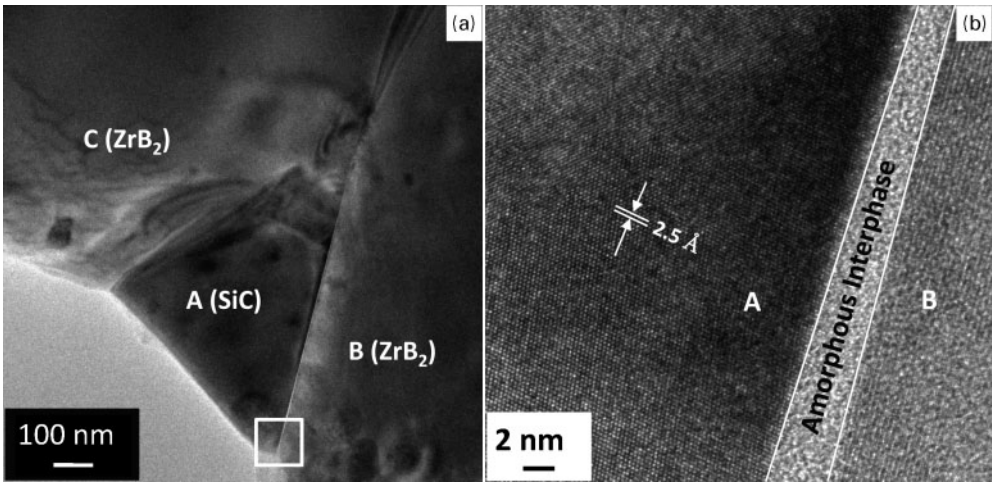

5 ***a*** **BF image of three-grain junction and** ***b*** **HRTEM image of grain boundary interphase taken from square region in** ***a***

β-Zr + ZrB_2→ZrB occurring between 1200 and 800°C on cooling. By diffusion of boron at the interface and through the peritectoid transformation, the intermediate ZrB phase is created as a buffer between the two low temperature phases preserving the high coherency of the interface. However, in our study, formation of β-Zr is highly unlikely even though the sintering was carried out in vacuum and hence the formation of ZrB through peritectoid transformation is not possible. In the event of forming a silicate or borosilicate melt during hot pressing, dissolution of ZrB_2 in the melt and precipitation of ZrB might be expected. However, the solubility of ZrB_2 is low in silicate melts and also the TEM investigation does not show such grain boundary interphase. Therefore the formation of ZrB might be attributed to the following reasons. Although XRD analyses did not show any crystalline oxide phase, EDS always revealed the presence of oxygen. With the presence of any adsorbed oxygen on the surface of SiC, thermodynamically both ZrB_2 and SiC will oxidise at high temperatures. It is believed that only boron in ZrB_2 receives oxygen forming B_2O_3 liquid and leaving behind boron-deficient zirconium boride. This is clearly demonstrated in the EDS analysis in Fig. 4 in that the cubic region contains less boron and more zirconia compared to ZrB_2. According to Aronsson,[53] in cases where ZrB has been observed, considerable O, C or N was present to stabilise the cubic structure, which is generally assumed to be the ZrB phase. In this study, the presence of impurities such as carbon, silicon and oxygen is most likely responsible for stabilising the formation of ZrB.

Conclusions

High resolution TEM observations reveal that *6H* α-SiC transforms into *3C* β- and *15R*-SiC and hexagonal ZrB_2 transforms into cubic ZrB in some regions of the hot pressed ZrB_2–SiC composites. Although these newly formed phases during hot pressing are only present in small amounts, they can significantly influence the high temperature mechanical properties and oxidation behaviour of the composites. The Burgers vectors of the observed dislocations in ZrB_2 are determined to be either $\mathbf{a}=\frac{1}{3}\langle 11\bar{2}0\rangle$ or $\mathbf{c}=\langle 0001\rangle$ using $\mathbf{g}\bullet\mathbf{b}$ criteria. The observations at interfaces revealed that there are no grain boundary phases.

Acknowledgements

One of the authors, DDJ thanks the Defence Science and Technology Laboratory (Dstl) for providing the financial support for this work under contract number DSTLX-1000015413. The authors kindly acknowledge use of the FEI TITAN 80–300 STEM facility at Imperial College London for HRTEM characterisation of interfaces.

References

1. M. A. Zhu and Y. G. Wang: 'Pressureless sintering ZrB_2–SiC ceramics at low temperatures', *Mater. Lett.*, 2009, **63**, (23), 2035–2037.
2. Q. Liu, W. N. Han, and P. Hu: 'Microstructure and mechanical properties of ZrB_2–SiC nanocomposite ceramic', *Scr. Mater.*, 2009, **61**, (7), 690–692.
3. X. H. Zhang, Z. Wang, P. Hu, W. B. Han, and C. Q. Hong: 'Mechanical properties and thermal shock resistance of ZrB_2–SiC ceramic toughened with graphite flake and SiC whiskers', *Scr. Mater.*, 2009, **61**, (8), 809–812.
4. J. Marschall, D. A. Pejakovic, W. G. Fahrenholtz, G. E. Hilmas, S. M. Zhu, J. Ridge, D. G. Fletcher, C. O. Asma and J. Thomel: 'Oxidation of ZrB_2–SiC ultrahigh-temperature ceramic composites in dissociated air', *J. Thermophys. Heat Transf.*, 2009, **23**, (2), 267–278.
5. S. C. Zhang, G. E. Hilmas and W. G. Fahrenholtz: 'Pressureless sintering of ZrB_2–SiC ceramics', *J. Am. Ceram. Soc.*, 2008, **91**, (1), 26–32.
6. S. C. Zhang, G. E. Hilmas, and W. G. Fahrenholtz: 'Pressureless densification of zirconium diboride with boron carbide additions', *J. Am. Ceram. Soc.*, 2006, **89**, (5), 1544–1550.
7. X. H. Zhang, L. Weng, J. Han, S. H. Meng and W. B. Han: 'Preparation and thermal ablation behavior of HfB_2–SiC-based ultra-high-temperature ceramics under severe heat conditions', *Int. J. Appl. Ceram. Technol.*, 2009, **6**, (2), 134–144.
8. L. Weng, X. H. Zhang, J. C. Han, W. B. Han and C. Q. Hong: 'The effect of B_4C on the microstructure and thermo-mechanical properties of HfB_2-based ceramics', *J. Alloys Compd*, 2009, **473**, (1–2), 314–318.
9. J. C. Han, P. Hu, X. H. Zhang, and S. H. Meng: 'Characteristics and mechanisms of dynamic oxidation for ZrB2–SiC based UHTC', *High-Perform. Ceram. V*, 2008, **368–372**, 1722–1726.
10. S. Q. Guo, Y. Kagawa, T. Nishimura, D. Chung and J. M. Yang: 'Mechanical and physical behavior of spark plasma sintered ZrC–ZrB_2–SiC composites', *J. Eur. Ceram. Soc.*, 2008, **28**, (6), 1279–1285.
11. Q. Qu, J. C. Han, W. B. Han, X. H. Zhang and C. Q. Hong: '*In situ* synthesis mechanism and characterization of ZrB_2–ZrC–SiC ultra high-temperature ceramics', *Mater. Chem. Phys*, 2008, **110**, (2–3), 216–221.
12. X. H. Zhang, Q. Qu, J. C. Han, W. B. Han and C. Q. Hong: 'Microstructural features and mechanical properties of ZrB_2–SiC–ZrC composites fabricated by hot pressing and reactive hot pressing', *Scr. Mater.*, 2008, **59**, (7), 753–756.
13. R. Licheri, R. Orru, C. Musa, A. M. Locci and G. Cao: 'Consolidation via spark plasma sintering of HfB_2/SiC and HfB_2/HfC/SiC composite powders obtained by self-propagating high-temperature synthesis', *J. Alloys Compd*, 2009, **478**, (1–2), 572–578.
14. D. Sciti, L. Silvestroni, S. Guicciardi, D. D. Fabbriche and A. Bellosi: 'Processing, mechanical properties and oxidation behavior of TaC and HfC composites containing 15 vol% $TaSi_2$ or $MoSi_2$', *J. Mater. Res.*, 2009, **24**, (6), 2056–2065.
15. H. B. Li, L. T. Zhang, L. F. Cheng and Y. G. Wang: 'Ablation resistance of different coating structures for C/ZrB_2–SiC composites under oxyacetylene torch flame', *International J. Appl. Ceram. Technol.*, 2009, **6**, (2), 145–150.
16. A. Pavese, P. Fino, C. Badini, A. Ortona and G. Marino: 'HfB_2/SiC as aprotective coating for 2D C-f/SiC composites: effect of high temperature oxidation on mechanical properties', *Surf. Coat. Technol.*, 2008, **202**, (10), 2059–2067.
17. G. Russo and G. Marino: 'The USV program and UHTC development', Proc. 4th Eur. Workshop on 'Hot structures and thermal protection systems for space vehicles', 29–38; 2003, Palermo, ESA Publications.
18. W. M. Guo, G. J. Zhang and P. L. Wang: 'Microstructural evolution and grain growth kinetics in ZrB_2–SiC composites during heat treatment', *J. Am. Ceram. Soc.*, 2009, **92**, (11), 2780–2783.
19. H. Zhang, Y. J. Yan, Z. R. Huang, X. J. Liu and D. L. Jiang: 'Properties of ZrB_2–SiC ceramics by pressureless sintering', *J. Am. Ceram. Soc.*, 2009, **92**, (7), 1599–1602.
20. T. Zhu, L. Xu, X. H. Zhang, W. B. Han, P. Hu and L. Weng: 'Densification, microstructure and mechanical properties of ZrB_2–SiCw ceramic composites', *J. Eur. Ceram. Soc.*, 2009, **29**, (13), 2893–2901.
21. T. Zhu, W. J. Li, X. H. Zhang, P. Hu, C. Q. Hong and L. Weng: 'Damage tolerance and R-curve behavior of ZrB_2–ZrO_2 composites', *Mater. Sci. Eng. A*, 2009, **A516**, (1–2), 297–301.
22. D. J. Chen, W. J. Li, X. H. Zhang, P. Hu, J. C. Han, C. Q. Hong and W. B. Han: 'Microstructural feature and thermal shock behavior of hot-pressed ZrB_2–SiC–ZrO_2 composite', *Mater. Chem. Phys.*, 2009, **116**, (2–3), 348–352.
23. J. Liang, C. Wang, Y. Wang, L. Jing and X. Luan: 'The influence of surface heat transfer conditions on thermal shock behavior of ZrB_2–SiC–AlN ceramic composites', *Scr. Mater.*, 2009, **61**, (6), 656–659.
24. X. H. Zhang, Z. Wang, X. Sun, W. B. Han and C. Q. Hong: 'Thermal shock behavior of ZrB_2–20 vol.% SiC–15 vol.% graphite

flake by hot pressing', *Int. J. Modern Phys. B*, 2009, **23B**, (6–7), 1160–1165.
25. W. J. Li, Y. Zhang, X. H. Zhang, C. Q. Hong and W. B. Han: 'Thermal shock behavior of ZrB_2–SiC ultra-high temperature ceramics with addition of zirconia', *J. Alloys Compd*, 2009, **478**, (1–2), 386–391.
26. W. M. Guo, G. J. Zhang, Y. M. Kan and P. L. Wang: 'Oxidation of ZrB_2 powder in the temperature range of 650–800°C', *J. Alloys Compd*, 2009, **471**, (1–2), 502–506.
27. T. A. Parthasarathy, R. A. Rapp, M. Opeka and R. J. Kerans: 'Effects of phase change and oxygen permeability in oxide scales on oxidation kinetics of ZrB_2 and HfB_2', *J. Am. Ceram. Soc.*, 2009, **92**, (5), 1079–1086.
28. C. M. Carney: 'Oxidation resistance of hafnium diboride-silicon carbide from 1400 to 2000°C', *J. Mater. Sci.*, 2009, **44**, (20), 5673–5681.
29. S. N. Karlsdottir and J. W. Halloran: 'Oxidation of ZrB_2–SiC: 'Influence of SiC content on solid and liquid oxide phase formation', *J. Am. Ceram. Soc.*, 2009, **92**, (2), 481–486.
30. S. J. Lee and D. K. Kim: 'The oxidation behavior of ZrB_2–based mixed boride', *SiAlONs Non-oxides*, 2009, **403**, 253–255.
31. G.-J. Zhang, Z.-Y. Deng, N. Kondo, J.-F. Yang and T. Ohji: 'Reactive hot pressing of ZrB_2–SiC composites', *J. Am. Ceram. Soc.*, 2000, **83**, (9), 2330–2332.
32. Y. Yan: 'Pressureless sintering of high-density ZrB_2–SiC ceramic composites', *J. Am. Ceram. Soc.*, 2006, **89**, (11), 3589–3592.
33. S. Hwang: 'Improved processing, and oxidation-resistance of ZrB_2 ultra-high temperature ceramics containing SiC nanodispersoids', *Mater. Sci. Eng. A*, 2007, **A464**, (1–2), 216–224.
34. W. W. Wu, G. J. Zhang, Y. M. Kan, P. L. Wang, K. Vanmeensel, J. Vleugels and O. van der Biest: 'Synthesis and microstructural features of ZrB_2–SiC-based composites by reactive spark plasma sintering and reactive hot pressing', *Scr. Mater.*, 2007, **57**, (4), 317–320.
35. F. Monteverde: 'Resistance to thermal shock and to oxidation of metal diborides-SiC ceramics for aerospace application', *J. Am. Ceram. Soc.*, 2007, **90**, (4), 1130–1138.
36. F. Monteverde and A. Bellosi: 'Oxidation of ZrB_2-based ceramics in dry air', *J. Electrochem. Soc.*, 2003, **150**, (11), B552–B559.
37. F. Monteverde and A. Bellosi: 'The resistance to oxidation of an HfB_2–SiC composite', *J. Eur. Ceram. Soc.*, 2005, **25**, (7), 1025–1031.
38. J. Han: 'Oxidation-resistant ZrB_2–SiC composites at 2200°C', *Compos. Sci. Technol.*, 2008, **68**, (3–4), 799–806.
39. J. W. Zimmermann, G. E. Hilmas, W. G. Fahrenholtz, F. Monteverde and A. Bellosi: 'Fabrication and properties of reactively hot pressed ZrB_2–SiC ceramics', *J. Eur. Ceram. Soc.*, 2007, **27**, (7), 2729–2736.
40. S. C. Zhang, G. E. Hilmas, and W. G. Fahrenholtz: 'Pressureless sintering of ZrB_2–SiC ceramics', *J. Am. Ceram. Soc.*, 2008, **91**, (1), 26–32.
41. V. M. Anishchik and N. N. Dorozhkin: 'Electronic structure of TiB_2 and ZrB_2', *Phys. Status Solidi B*, 2006, **160B**, (1), 173–177.
42. W. Y. Ching, Y. N. Xu, P. Rulis and L. Ouyang: 'The electronic structure and spectroscopic properties of 3C, 2H, 4H, 6H, 15R and 21R polymorphs of SiC', *Mater Sci. Eng. A*, 2006, **A422**, 147–156.
43. L. Geng and J. Zhang: 'A study of the crystal structure of a commercial b-SiC whisker by high-resolution TEM', *Mater. Chem. Phys.*, 2004, **84**, (2–3), 243–246.
44. M. M. Hong: 'Stacking fault energy of 6H-SiC and 4H-SiC single crystals', *Philos. Mag. A*, 2000, **80A**, (4), 919.
45. A. A. Gunnaes: 'Morphology and structure of airborne β-SiC fibres produced during the industrial production of non-fibrous silicon carbide', *J. Mater. Sci.*, 2005, **40**, (22), 6011.
46. Y. Champion and S. Hagege: 'HREM analysis of a cubic-hexagonal (ZrB–ZrB_2) interface using the coincidence approach', *Acta Mater.*, 1997, **45**, (6), 2621–2631.
47. Y. Champion, S. Hagege and M. Masse: 'Structural analysis of phases and heterophase interfaces in the zirconium-boron system', *J. Mater. Sci.*, 1998, **33**, (16), 4035–4041.
48. Y. Champion and S. Hagege: 'Experimental determination and symmetry related analysis of orientation relationships in hetero-phase interfaces: a case study in the Zr–B system', *Acta Mater.*, 1996, **44**, (10), 4169–4179.
49. P. E. A. R. Kieffer, E. Gugel and A. Schmidt: *Mater. Res. Bull.*, 1968, **4**, 153.
50. P. Kackell, J. Furthmuller and F. Bechstedt: 'Polytypic transformations in SiC: an *ab initio* study', *Phys. Rev. B*, 1999, **60B**, (19), 13261–13264.
51. P. P. Pirouz: 'Polytypic transformations in silicon carbide: the role of TEM', *Ultramicroscopy*, 1993, **51**, (1), 189.
52. S. I. Vlaskina and D. H. Shin: '6H to 3C polytype transformation in silicon carbide', *Jpn J. Appl. Phys.*, 1998, **38**, L27–L29.
53. Y. Champion and S. Hagege: 'A study of composite interfaces in the Zr–ZrB_2 system', *J. Mater. Sci. Lett.*, 1992, **11**, 290–293.